

Dynamics of radiating particles in current sheets with a transverse magnetic field component

A. Muraviev^{1,*}

¹*Institute of Applied Physics of the Russian Academy of Sciences, Nizhny Novgorod 603950, Russia*

(Dated: May 13, 2022)

Current sheets in the vicinity of pulsars or those predicted on upcoming multipetawatt laser facilities can feature extremely high electromagnetic fields. As a result, charged particles in such sheets may experience significant radiation losses. We present an analysis of particle motion in model fields of a relativistic neutral current sheet with two magnetic field components in the case when radiative effects must be accounted for. In the Landau-Lifshitz radiation reaction model the method of slowly changing parameters is used to quantify the influence of radiative effects. A quasiadiabatic invariant of dissipative motion is found. It is shown how the presented method can be used in a wider range of problems.

I. INTRODUCTION

Current sheets are magnetoplasma structures that both exist naturally in the Universe and can be formed in laboratory experiments. Much attention has been paid to current sheets of various structure and origin, for example, those forming as a result of solar wind interaction with planetary magnetic fields. In most of these cases the characteristic values of magnetic fields and particle energies do not require the consideration of radiation losses, and analytical solutions of equations of particle motion in such structures were obtained [1–8].

However, for current sheets formed under extreme conditions radiation losses due to abundant photon emission can play a significant role in particle dynamics. Such extreme conditions can be natural, for example those in the vicinity of pulsars [9], or be a result of extreme laser-plasma interaction [10, 11] in experiments on modern or upcoming multipetawatt laser facilities [12]. Earlier works show that radiative effects can significantly affect both individual and collective particle dynamics [13–21].

In the work [7] the dynamics of particles in a null current sheet with a fixed *two-component magnetic field* was studied *without the consideration of relativism or radiation losses*. The primary component of the magnetic field is considered to be parallel to the sheet and to linearly depend on the distance to the sheet (the center of the sheet being the null point), and the secondary component is considered to be constant and perpendicular to the sheet. In a recent work the influence of *radiation losses* was investigated theoretically and numerically for *ultra-relativistic* particles in a *single-component fixed magnetic field* [22], this quasistationary plasma-field configuration is similar to laser excited [10, 11] and space current sheets [1, 2, 6, 9, 23]. The goal of the current work is to combine the results of works [7] and [22] and study the dynamics of *ultrarelativistic* particles experiencing *weak radiation losses* in a more general *two-component configuration of the magnetic field*.

Although current sheets are complicated self-consistent plasma-field structures and particle dynamics should ideally be considered self-consistently with the field generated by all particles, the focus of this paper is the influence of radiation losses on particle dynamics. Therefore, in this paper we study the motion of probe particles experiencing radiation losses in a fixed two-component magnetic field modeling the field structure of a current sheet.

In our study we consider the case when a relativistic particle emits photons frequently and each emitted photon carries away a negligible part of particle energy, so it is reasonable to consider radiation losses in the form of the Landau-Lifshitz (LL) force [24]. In the case of weak radiative reaction we quantify its influence on the dynamics of particles and find a quasiadiabatic invariant of dissipative motion.

The structure of this paper is as follows. In Section II we rederive some of the results of the work [7] in the relativistic case and offer a way to deal with significantly different time scales of interdependent features of particle dynamics. In Section III we consider radiation reaction in the form of a continuous force of radiative friction in the Landau-Lifshitz form and use the method of slowly changing parameters to study the dynamics of particles with this force taken into account. In Section IV we discuss how some of the assumptions we had employed can be lifted and show how this method can be applied to a wider range of problems.

II. BASE MODEL

In this section we consider *without radiation losses* the motion of a *relativistic* positron in a constant inhomogeneous magnetic field with two non-zero components

$$\begin{cases} B_y(x) = kx \\ B_x = \text{const} \end{cases}, \quad (1)$$

and an according vector potential $A_z(x, y) = B_x y - kx^2/2$. The motion of an electron is symmetrical and can be derived by replacing e with $-e$.

* sashamur@gmail.com

Particle motion in a field of such configuration has been studied before in [2, 4, 7] in the non-relativistic case. It was shown that in the case when $B_x \ll B_{y_{max}}$ the motion can be considered as a superposition of two motions. The "slow" quasi-closed-loop motion near the sheet plane $x = 0$ is due to the magnetic field component B_x perpendicular to the sheet, this motion can be considered in the phase space (y, p_y) . The "fast" oscillations in the transverse direction are due to the B_y component, which has a null point in the center of the sheet. This motion can be considered in the phase space (x, p_x) [7].

We intend to show that in this problem relativity can be accounted for with rather minor adjustments. The key factor here is that, since the field is purely magnetic and in this section we are not considering radiation losses yet, the kinetic energy and the Lorentz-factor γ of the particle remain constant, as well as the absolute values of momentum p and velocity V , any of which can be considered the first integral of motion.

Additionally, for this system a second integral of motion can be obtained: since the vector-potential $A = (0, 0, A_z(x, y))$ does not depend on z , it is evident that $P_z = p_z + eA_z/c = const$, where P is the generalized momentum, $e > 0$ is the positron charge, and c is the speed of light. Therefore, $p_z = P_z - e(B_x y - kx^2/2)/c$. Using this expression, the system of equations for the motion of the particle can be written as:

$$\begin{cases} \dot{x} = p_x/m\gamma \\ \dot{y} = p_y/m\gamma \\ \dot{z} = p_z/m\gamma \\ \dot{p}_x = -\frac{e}{c}kxp_z/m\gamma \\ \dot{p}_y = \frac{e}{c}\dot{B}_x p_z/m\gamma \\ p_z = P_z - \frac{e}{c}(B_x y - \frac{kx^2}{2}) \end{cases}, \quad (2)$$

where m is the positron mass. Due to the conservation of total momentum the system of equations is similar to the non-relativistic one with the exception of the $1/\gamma$ factor.

From this system we can extract the systems of equations for "fast" and "slow" motion, respectively:

$$\begin{cases} \dot{x} = p_x/m\gamma \\ \dot{p}_x = -\frac{e}{c}kx(P_z - \frac{e}{c}(B_x y - \frac{kx^2}{2}))/m\gamma \end{cases}, \quad (3)$$

$$\begin{cases} \dot{y} = p_y/m\gamma \\ \dot{p}_y = \frac{e}{c}B_y(P_z - \frac{e}{c}(B_x y - \frac{kx^2}{2}))/m\gamma \end{cases}. \quad (4)$$

As we can see, these systems are not completely separable, i.e. \dot{p}_y depends on x , and \dot{p}_x depends on y . However, the assumption of significantly different timescales for the "fast" and the "slow" motion allows us to separate them.

For the sake of "fast" motion y and p_y are "frozen" external parameters. Thus, the conservation of momentum during "fast" motion can be written as $p_x^2 + p_z^2 = p^2 - p_y^2 = const$ [7], since p_y does not change on the "fast" time scale. Then the parameter η from [22] (or $-s$ from [7]) that determines the type of motion in the

"fast" phase space (x, p_x) can be written as

$$\eta(y, p_y) = (P_z - eB_x y/c)/\sqrt{p^2 - p_y^2} \quad (5)$$

[25]. In the work [22] η was the second integral of motion as there was no y or p_y . In this work, however, the point on the "slow" (y, p_y) plane corresponds to and determines the trajectory on the "fast" (x, p_x) plane.

For the sake of "slow" motion the terms depending on the "fast" variable x can be averaged over the period of "fast" motion, and the averaged values are functions of (y, p_y) , which can be computed with the help of the results of [22]. For example, as follows from [22] Eq.2,

$$\overline{x^2} = \frac{2c}{ek} p \sqrt{1 - q_y^2} (\overline{\cos \varphi} - \eta), \quad (6)$$

where $q_y \equiv p_y/p$ [26] and φ is the "fast" motion direction of propagation (projected onto the xz plane): $\sin \varphi = p_x/p_{xz}$, $\cos \varphi = p_z/p_{xz}$. The value $\overline{\cos \varphi}$ can be computed as

$$\overline{\cos \varphi} = \frac{\int_{T_x} \cos \varphi dt}{\int_{T_x} dt} = \frac{\int_0^{\varphi_{max}} (\cos \varphi / \dot{\varphi}) d\varphi}{\int_0^{\varphi_{max}} (1/\dot{\varphi}) d\varphi}.$$

Since $\dot{\varphi} = \sqrt{2ek/m\gamma} \sqrt{\cos \varphi - \eta}$ [22],

$$\overline{\cos \varphi} = \frac{\int_0^{\varphi_{max}} \frac{\cos \varphi}{\sqrt{\cos \varphi - \eta}} d\varphi}{\int_0^{\varphi_{max}} \frac{1}{\sqrt{\cos \varphi - \eta}} d\varphi},$$

which with the help of the substitution $\sin \alpha = \sin(\varphi/2)/\sqrt{(1-\eta)/2}$ can be computed as

$$\overline{\cos \varphi} = \begin{cases} 2 \frac{E[(1-\eta)/2]}{K[(1-\eta)/2]} - 1, \eta > -1 \\ \eta - (1+\eta) \frac{E[2/(1+\eta)]}{K[2/(1+\eta)]}, \eta < -1 \end{cases}, \quad (7)$$

where K, E are complete elliptic integrals of the first and second kind, respectively, and η is a function of (y, p_y) as defined in (5). The notation

$$\begin{cases} K[\kappa^2] = \int_0^{\pi/2} d\varphi / \sqrt{1 - \kappa^2 \sin^2 \varphi} \\ E[\kappa^2] = \int_0^{\pi/2} d\varphi \sqrt{1 - \kappa^2 \sin^2 \varphi} \end{cases} \quad (8)$$

is used.

In theory equations (6) and (7) allow excluding the term x^2 from (4), but one can see that even then solving (4) directly would be problematic. In order to study the system (4), we employ the quasiadiabatic invariant [7]:

$$i_x(y, q_y) = \frac{1}{2\pi} (1 - q_y^2)^{3/4} f(-\eta), \quad (9)$$

where

$$f(s) = \begin{cases} \frac{2}{3} (K[\kappa^2](1-s) + 2sE[\kappa^2]), -1 \leq s \leq 1 \\ \frac{4}{3} \kappa (K[\kappa^{-2}](1-s) + sE[\kappa^{-2}]), s \geq 1 \end{cases} \quad (10)$$

and $\kappa = \sqrt{(1+s)/2}$. Unlike the work [7], in our notation i_x is dimensionless.

Each possible value of i_x corresponds to a closed loop on the (y, q_y) plane, the possible values are $0 < i_x < i_{xmax} \equiv f_{max}/(2\pi) \approx 0.246$, where $f_{max} \approx 1.55$ is the maximal value of the function $f(s)$. i_x is well conserved along the trajectory except in the vicinity of the *uncertainty curve* (in red on Fig. 2) determined by $\eta(y, q_y) = -1$, where it experiences a quasirandom jump [7]. Since this paper is devoted to studying the influence of radiation losses on the trajectory, and not much radiation loss is accumulated in the small vicinity of the uncertainty curve where the jump occurs, the quasirandom jumps of the quasiadiabatic invariant will be disregarded throughout this paper unless specifically stated otherwise. The green curve on Fig. 2 is the curve $\dot{q}_y = 0$ or $\eta(y, q_y) = \eta^*$ [22], which will be important later. To the left of the green curve $\eta^* < \eta(y, q_y) \leq 1$ and the "fast" trajectory is of type A or B [22] (meandering). Between the green and the red curves $-1 < \eta(y, q_y) < \eta^*$ and the trajectory is of type C [22]. To the right of the red curve $\eta(y, q_y) < -1$ and the trajectory is of type D [22] (non-crossing).

An interesting feature of this system is that $\dot{z} \sim p_y \sim p_z$. As a result, with the right choice of the origin of coordinates $z \sim p_y$, and the trajectory in the phase space (y, p_y) is similar to the projection of the trajectory onto the yz plane. In the x direction the trajectory oscillates around zero if the current point on the (y, p_y) plane is to the left of the red curve and around a non-zero value with a quasirandom sign [7, 22] if it is to the right of the red curve. Thus, the whole trajectory resembles a split torus.

III. IMPLEMENTING RADIATIVE RECOIL

A positron moving along a curvilinear trajectory can emit photons. Based on the preceding works [11, 22] we allow the magnetic field and particle energy values to be sufficiently high in order for the particles to exhibit radiative recoil. Even though a single impact experienced by the particle as a result of photon emission can be rela-

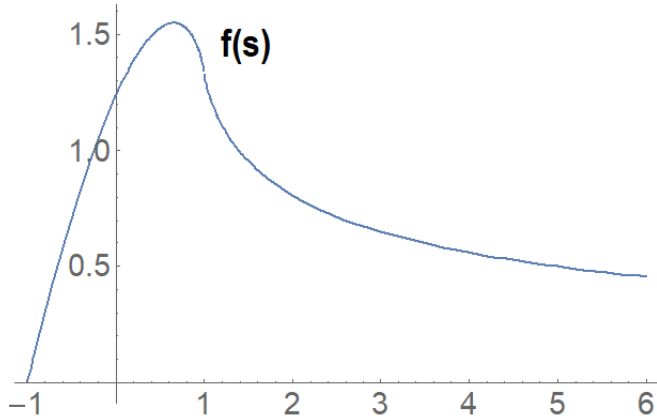


FIG. 1. The function $f(s)$.

tively weak, particle motion can be qualitatively modified as a result of a sequence of such acts. While recoil-free motion of particles would be infinite and quasiperiodic as described in Sec.II, even recoil insignificant over one period of particle motion due to photon emission may accumulate over multiple periods and have a significant effect on the motion of particles. In the work [11] current sheets are shown to be formed by ultraintense laser fields. The lifetime of these current sheets was observed to be much larger than the laser wave period, which is in turn much greater than the characteristic times of particle trajectories, so such an accumulation may indeed take place.

In this section we consider particle motion in the field structure with two non-zero components $B_y(x) = kx$ and $B_x = \text{const}$ with radiative recoil. In the case when particles emit photons often and they carry away a negligible part of the particle's energy, it is reasonable to consider radiation losses in the form of a continuous Landau-Lifshitz friction force [24]. We also consider only the ultrarelativistic case $p/mc \approx \gamma \gg 1$, which allows us to neglect the first and second terms of the LL force [24]. In our setup this translates to:

$$\vec{F}_{rad} = -\frac{2e^4 \vec{V}}{3m^2 c^7} \gamma^2 [V \times B]^2, \quad (11)$$

or, after expanding the vector product,

$$\vec{F}_{rad} = -\frac{2e^4 \vec{V}}{3m^2 c^7} \gamma^2 [k^2 x^2 (1 - q_y^2) + B_x^2 (1 - (1 - q_y^2) \sin^2 \varphi)]. \quad (12)$$

In Sec. II γ was constant as there was no recoil/friction. Accounting for radiative friction forces us to treat γ as another parameter depending on time. Like in [22], we will use the variable $\mu = 1/\gamma$ as the main variable characterizing the current energy. Taking into account that particle energy decreases due to radiative friction given by the LL force in Eq. (12), the equation for $\dot{\mu} = \frac{d\mu}{dt}$ can be written as:

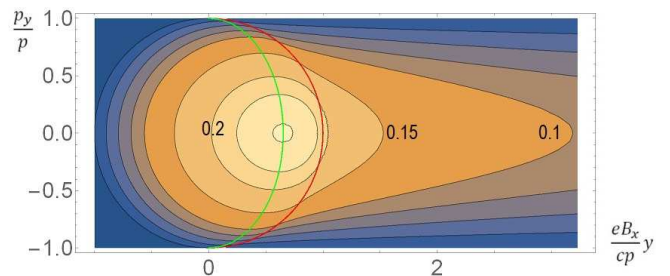


FIG. 2. The phase space of "slow" variables (y, q_y) . The uncertainty curve is shown in red. The green curve represents $\dot{p}_y = 0$. Trajectories are denoted with the corresponding value of i_x .

$$\dot{\mu} = \frac{2e^4}{3m^3c^5} [k^2x^2(1 - q_y^2) + B_x^2(1 - (1 - q_y^2)\sin^2\varphi)]. \quad (13)$$

Thus, the main parameters characterizing the state of the particle are μ (determines the particle's energy) and i_x (determines what trajectory the particle is on in the (y, p_y) phase space). (y, p_y) determine at which point of that trajectory that particle is at the moment, and the shape of the potential the particle oscillates in, as well as the particle's energy, in the (x, p_x) phase space. It is important that (y, p_y) are not independent considering a given i_x . And finally, x or φ determines at which point of that "fast" potential the particle is at the moment.

Our primary objective is to study the influence of *weak* radiative friction, so we will assume that

$$T_x \ll T_y \ll \frac{\mu}{\dot{\mu}}, \frac{i_x}{\dot{i}_x}. \quad (14)$$

The positron's motion at any given moment of time can be approximated by the solution for the case without radiative friction, and we treat μ and i_x as slowly changing parameters. In order to account for radiative friction, we must quantify its influence on these parameters over the half-period of motion in the (y, p_y) plane $T_y/2$, and find how that quantity depends on μ and i_x .

To quantify $\Delta\mu$ we integrate $\dot{\mu}(\mu, i_x)$ over $T_y/2$. In order to do that, we use $d\mu/dq_y = \dot{\mu}/\dot{q}_y$ and integrate over q_y instead. Here, from (2) and (6),

$$\begin{aligned} \dot{q}_y &= \frac{eB_x\mu}{mc} \left((P_z - \frac{e}{c}B_x y) + \frac{ekx^2}{2c} \right) / p = \\ &= \frac{eB_x\mu}{mc} \left(\eta \sqrt{1 - q_y^2} + \sqrt{1 - q_y^2}(\cos\varphi - \eta) \right) = \\ &= \frac{eB_x\mu}{mc} \sqrt{1 - q_y^2} \cos\varphi \end{aligned} \quad (15)$$

However, since η in the expression for $\dot{\mu}$ (13) depends on both y and $q_y \equiv p_y/p$ (5), it must first be written as a function of i_x and q_y instead. Both pairs of variables are valid ways of representing a point on the (y, p_y) plane [27]. Note that radiative friction is not inflicted onto q_y , since the force (11) is always directed against the particle's velocity. As such, η must be written as:

$$\eta(i_x, q_y) = -f^{-1}(2\pi i_x(1 - q_y^2)^{3/4}), \quad (16)$$

as follows from (9). Here, f^{-1} is the inverse function of f .

For simplicity here we will recall that we consider B_x to be weak [7] and neglect the second term of (13). Then, $\Delta\mu$ can be written as:

$$\Delta\mu(\mu, i_x) = \frac{4e^2k}{3mc^2B_x\mu^2} \oint_{i_x} (1 - q_y^2)(1 - \eta/\overline{\cos\varphi(\eta)}) dq_y, \quad (17)$$

where $\eta = \eta(i_x, q_y)$ according to (16) and $\overline{\cos\varphi(\eta)}$ is a function of η according to (7). The integral is performed over a closed-loop trajectory on (y, p_y) , on which $i_x = \text{const}$. For parts of the trajectory when $\dot{q}_y > 0$ (to the left of the green curve on Fig. 2) the lower branch of the two-valued function f^{-1} should be used. When $\dot{q}_y < 0$ (to the right of the green curve on Fig. 2), its upper branch should be used.

As a result, the integral is broken up into two parts for trajectories not crossing the *uncertainty curve*, those have i_x in the interval $0.212 \approx 2/3\pi \equiv i_x^* < i_x < i_{x\max} \equiv f_{\max}/2\pi \approx 0.246$ [28], and into three parts for trajectories crossing the *uncertainty curve* ($0 < i_x < i_x^*$) because of the piecewise properties of the functions $f(s)$ and $\overline{\cos\varphi(\eta)}$. The limits of integration can be found by substituting $\eta = \eta^* \approx -0.65$, where $f(-\eta^*) = f_{\max}$ (also see [22]), for the green curve, and $\eta = -1$ for the red curve into (9) and solving for q_y :

$$q_y = \pm \sqrt{1 - \left(\frac{2\pi i_x}{f(-\eta)} \right)^{4/3}}. \quad (18)$$

Note that in these variables the integrable part of (17) depends only on i_x , while all dependence on μ can be factored out of the integral. As a result, $\Delta\mu(\mu, i_x)$ can be written as a product of two functions with separated variables: $\Delta\mu(\mu, i_x) = F_\mu(\mu)G_{i_x}(i_x)$. In this case we can define $F_\mu(\mu) = 4e^2k/3mc^2B_x\mu^2$, then

$$F_{i_x}(i_x) = \oint_{i_x} (1 - q_y^2)(1 - \eta/\overline{\cos\varphi(\eta)}) dq_y, \quad (19)$$

where, again, $\eta = \eta(i_x, q_y)$ according to (16) and $\overline{\cos\varphi(\eta)}$ is a function of η according to (7). We will see momentarily that the same thing applies to Δi_x , which can be written as $\Delta i_x(\mu, i_x) = G_\mu(\mu)G_{i_x}(i_x)$.

Since any change in the quasiadiabatic invariant i_x is a direct consequence of radiative friction, \dot{i}_x can be calculated as $\dot{i}_x = \frac{di_x}{d\mu}\dot{\mu}$, where $\frac{di_x}{d\mu}$ can be derived from (9):

$$\frac{di_x}{d\mu} = -\frac{1}{2\pi}(1 - q_y^2)^{3/4}f'(-\eta)\frac{\eta}{\mu}. \quad (20)$$

Accordingly, the expression for the change of i_x over the half-period $T_y/2$ can be expressed as:

$$\Delta i_x = -\frac{G_\mu(\mu)}{2\pi} \oint_{i_x} (1 - q_y^2)^{7/4} \eta f'(-\eta)(1 - \eta/\overline{\cos\varphi(\eta)}) dq_y, \quad (21)$$

keeping in mind (16) and (7). Here we chose $G_\mu(\mu) = -4e^2k/3mc^2B_x\mu^3$ or

$$G_\mu(\mu) = F_\mu(\mu)/\mu, \quad (22)$$

while

$$G_{i_x}(i_x) = -\frac{1}{2\pi} \oint_{i_x} (1 - q_y^2)^{7/4} \eta f'(-\eta)(1 - \eta/\overline{\cos\varphi(\eta)}) dq_y; \quad (23)$$

(16), (7).

The functions $F_{i_x}(i_x)$ and $G_{i_x}(i_x)$ are quite hard to calculate do to the implicit definition of f^{-1} and piecewise properties of many underlying functions, but we have now reduced them to dimensionless functions of a single variable, which means *they can be calculated once and tabulated* with any required precision.

Moreover, if we consider timescales much larger than T_y , the expressions $\frac{\Delta\mu}{T_y/2}$ and $\frac{\Delta i_x}{T_y/2}$ can be viewed as differential equations $\dot{\mu}$ and \dot{i}_x , respectively:

$$\begin{cases} \dot{\mu}(\mu, i_x) = \frac{F_\mu(\mu)F_{i_x}(i_x)}{T_y/2} \\ \dot{i}_x(\mu, i_x) = \frac{G_\mu(\mu)G_{i_x}(i_x)}{T_y/2} \end{cases} \quad (24)$$

But in that case there exists an invariant $L(\mu, i_x) = L_\mu(\mu)L_{i_x}(i_x)$. From $\frac{d}{dt}L(\mu, i_x) = 0$ follows $L'_\mu(\mu)L_{i_x}(i_x)F_\mu(\mu)F_{i_x}(i_x) + L_\mu(\mu)L'_{i_x}(i_x)G_\mu(\mu)G_{i_x}(i_x) = 0$ or:

$$\frac{L'_\mu(\mu)F_\mu(\mu)}{L_\mu(\mu)G_\mu(\mu)} = -\frac{L'_{i_x}(i_x)G_{i_x}(i_x)}{L_{i_x}(i_x)F_{i_x}(i_x)} = const, \quad (25)$$

since the left side does not depend on i_x and the right side does not depend on μ .

In that case due to Eq. 22 it is easily found that

$$L_\mu = \exp\left(\int \frac{G_\mu(\mu)}{F_\mu(\mu)}d\mu\right) = \mu. \quad (26)$$

$$L_{i_x} = \exp\left(-\int \frac{F_{i_x}(i_x)}{G_{i_x}(i_x)}di_x\right). \quad (27)$$

We will use Eq. 27 to find L_{i_x} for all i_x in the following subsection. But for trajectories with $i_x \ll i_{xmax}$ it can be estimated independently of Eq. 27 that $L_{i_x} = i_x^2$. Indeed, since $\dot{p}_y \sim \dot{z}$, and $|\dot{z}|$ is very small on the near-Larmor trajectories with $-\eta \gg 1$ (to the right of the red curve on Fig. 2) [4, 22], a particle spends a lot more time with $\dot{p}_y < 0$ (to the right of the green curve) than with $\dot{p}_y > 0$ (to the left of the green curve). Additionally, its average x^2 is also larger [4, 7, 22], and therefore so is its exposure to radiative friction. Therefore, for a rough estimate the influence of weaker radiative friction over shorter periods of time to the left of the red curve can be neglected, and only the part of the trajectory to the right of the red curve can be considered. Finally, remembering that $i_x \sim \oint p_x dx / p^{3/2}$ [7], the Larmor radius in the ultrarelativistic case $R_L \sim \gamma$ and $p \sim \gamma$, it can be concluded that $i_x \sim \gamma^{1/2} = \mu^{-1/2}$, thus $i_x^2 \mu \approx const$.

A. The functions $\Delta\mu(i_x)$, $\Delta i_x(i_x)$ and $L(i_x)$

At this point the μ -dependent parts of the discussed functions have been identified, so we will refer to F_{i_x} as μ , to G_{i_x} as i_x and to L_{i_x} as L to underline their physical

meaning. In this subsection we will present the results of numerical calculations of the specified functions, as well as fits for these functions in different regions, and discuss the inferences.

1. $\Delta\mu(i_x)$

Using asymptotic expressions for the underlying functions in the case $i_x \ll i_{xmax}$ and $-\eta \gg 1$ a dependence $\Delta\mu \sim i_x^{-4}$ can be derived, so we expect to see $\Delta\mu i_x^4 \approx const$ near $i_x = 0$.

The graph of $\Delta\mu(i_x)$ is shown in Fig. (3). It is indeed evident that $\Delta\mu i_x^4 = const$ is a good approximation for $i_x \ll i_{xmax}$ and it holds a better than 1% precision for $i_x < 0.15$. Note that the function has a breaking point near $i_x = i_x^* \approx 0.212$, which corresponds to the trajectory on Fig.2 tangent to the red curve.

2. $\Delta i_x(i_x)$

Using the approximate invariant $L \approx \mu i_x^2$, or using asymptotic expressions for the underlying functions in the case $i_x \ll i_{xmax}$ and $-\eta \gg 1$, a dependence $\Delta\mu \sim i_x^{-3}$ can be derived, so we expect to see $i_x^3 \Delta i_x \approx const$ near $i_x = 0$. Note that Δi_x is negative, so the graph depicts the value $-\Delta i_x$.

The graph of $-\Delta i_x(i_x)$ is shown in Fig. (4). It is indeed evident that $i_x^3 \Delta i_x = const$ is a good approximation for $i_x \ll i_{xmax}$. The rough fit near $i_x = i_{xmax}$ (in red) was obtained numerically and is $-\Delta i_x = 4.4(i_{xmax} - i_x) - 18(i_{xmax} - i_x)^2$.

3. $\Delta\mu(i_x)/\Delta i_x(i_x)$

The function $\Delta\mu(i_x)/\Delta i_x(i_x)$ or $F_{i_x}(i_x)/G_{i_x}(i_x)$ is crucial for the calculation of the invariant L according to Eq.27. The graph depicts the negated value $-\Delta\mu(i_x)/\Delta i_x(i_x)$, or $-\Delta\mu/\Delta i_x$. $-\Delta\mu/\Delta i_x \approx 2/i_x$ is expected near $i_x = 0$.

The graph of $-\Delta\mu(i_x)/\Delta i_x(i_x)$ is shown in Fig. 5. The expected fit $2/i_x$ at $i_x \ll i_{xmax}$ works well, a more precise one obtained numerically and used in Fig. 5 in green is $2/i_x - 430i_x^{5/2}$. Near $i_x = i_{xmax}$ the linear character of $-\Delta i_x$ on Fig.4 and the roughly constant character of $\Delta\mu$ on Fig.3 suggest a very rough fit can be made, shown in red and equal to $0.62/(i_{xmax} - i_x)$. On subplot (b) in the logarithmic scale a breaking point near $i_x = i_x^*$ is once again evident.

4. $L(i_x)$

The function $L(i_x)$ is obtained numerically using expression (27). $L \approx i_x^2$ is expected at $i_x \ll i_{xmax}$.

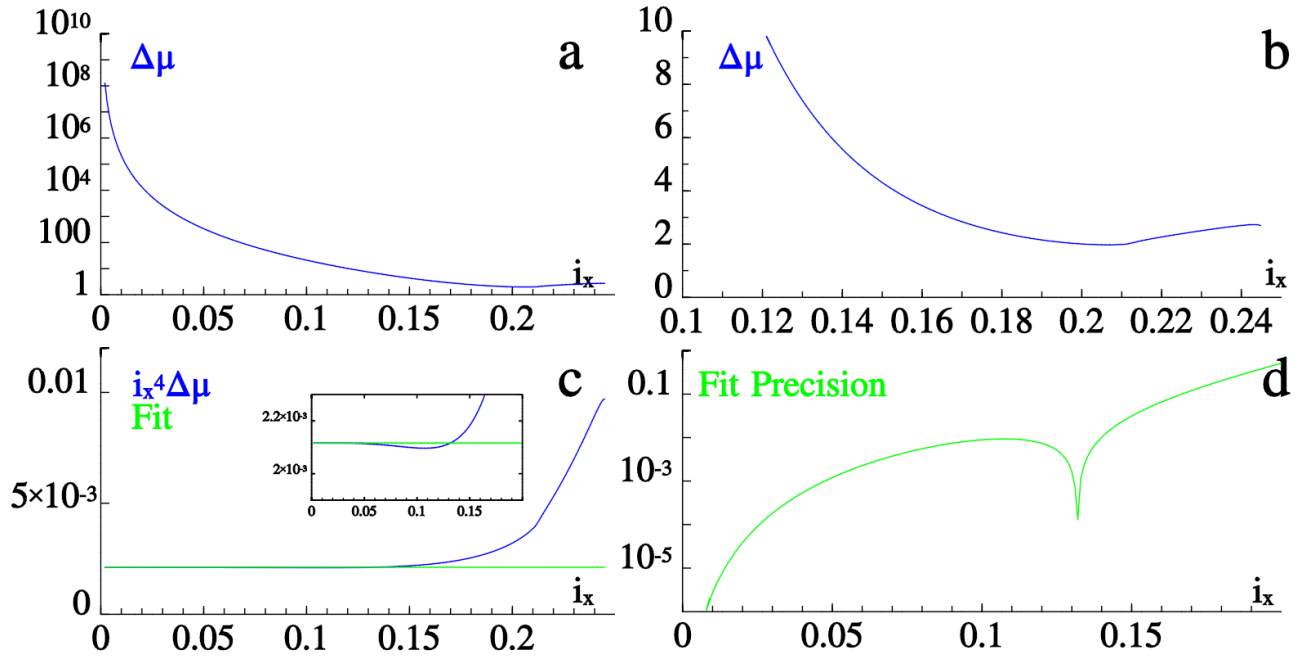


FIG. 3. (a) $\Delta\mu(i_x)$ on a logarithmic scale. (b) The lower part of $\Delta\mu(i_x)$ ($i_x > 0.1$) on a linear scale. (c) $\Delta\mu i_x^4(i_x)$ (blue) and its fit (green), in this case a constant. (d) Accuracy of the fit on a logarithmic scale.

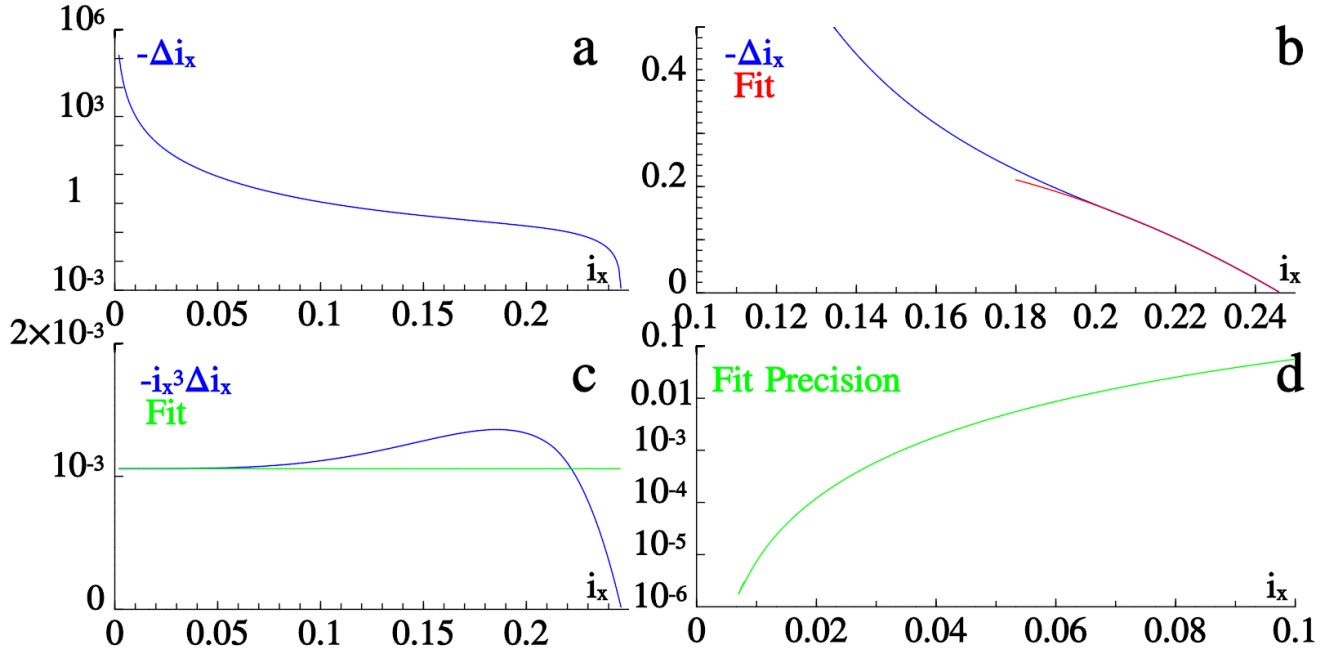


FIG. 4. (a) $-\Delta i_x(i_x)$ on a logarithmic scale. (b) The lower part of $-\Delta i_x(i_x)$ ($i_x > 0.1$) on a linear scale (blue), its rough fit by a quadratic function (red). (c) $-i_x^3 \Delta i_x$ (blue) and its fit (green), in this case a constant. (d) Accuracy of the fit on a logarithmic scale.

The graph of $L(i_x)$ is shown in Fig. 6. The expected fit $L \approx i_x^2$ at $i_x \ll i_{xmax}$ works well, a more precise one used in Fig. 6 is $L = i_x^2 - 110i_x^{11/2}$. As follows from the fit to $\Delta\mu(i_x)/\Delta i_x(i_x)$, a rough fit can be made near $i_x = i_{xmax}$, shown in red and equal to $5 \cdot 10^{-3}(i_{xmax} - i_x)^{-0.62}$.

5. Takeaways

In the assumptions of weak radiative friction (14) and ultrarelativity ($\gamma \gg 1$ or $\mu \ll 1$) the motion of particles in current sheets with the field structure (1) was

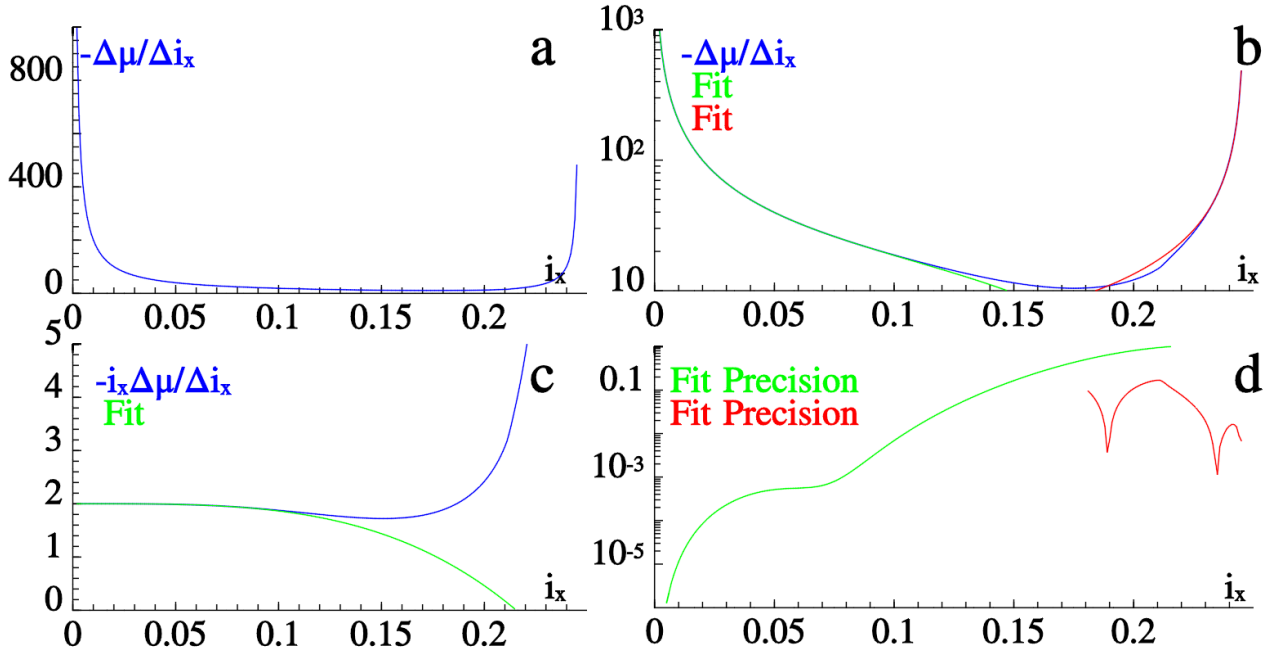


FIG. 5. (a) $-\Delta\mu(i_x)/\Delta i_x(i_x)$ on a linear scale. (b) $-\Delta\mu(i_x)/\Delta i_x(i_x)$ on a linear scale (blue), its fits at $i_x \ll i_{xmax}$ (green) and near $i_x = i_{xmax}$ (red). (c) $-i_x \Delta\mu(i_x)/\Delta i_x(i_x)$ (blue) and its fit at $i_x \ll i_{xmax}$ (green). (d) Accuracy of the fits on a logarithmic scale.

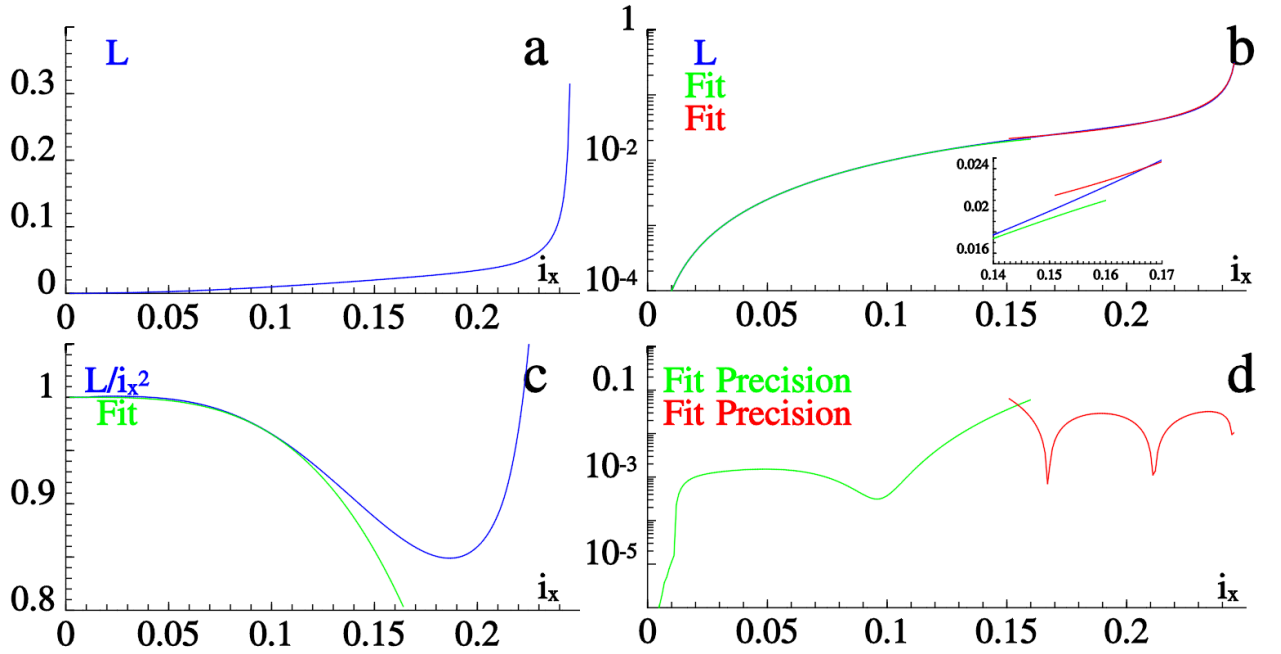


FIG. 6. (a) $L(i_x)$ on a linear scale. (b) $L(i_x)$ on a logarithmic scale (blue), its fits at $i_x \ll i_{xmax}$ (green) and near $i_x = i_{xmax}$ (red). (c) $L(i_x)/i_x^2$ (blue) and its fit at $i_x \ll i_{xmax}$ (green). (d) Accuracy of the fits on a logarithmic scale.

studied. It is also assumed that the field component B_x contributes only to the shape of the unperturbed trajectory, making it 3D instead of 2D [4, 7, 22], but does not contribute to radiative friction. Since the former is a qualitative change and the latter is a quantitative contribution, such assumptions can be justified in the case

when B_x is sufficiently weak [7].

Within these assumptions the main parameters defining the trajectory (μ and i_x), being integrals of motion in the frictionless case, are now considered as slowly changing parameters. In order to quantify the influence of radiative friction, the change in these parameters due to

radiative friction is integrated over a half-period $T_y/2$ of the unperturbed trajectory. The exact expressions even within our assumptions are rather intricate (See Eqs.(17),(21),(16),(10),(7),(8)), mostly owing to the implicit definition of the dual-branch function f^{-1} and the piecewise properties of f^{-1} and other underlying functions. Thus, the required functions have been nondimensionalized and calculated numerically.

The analytical approximations made in the limit $i_x \ll i_{xmax}$ work well up to at least $i_x \approx 0.05$, some up to $i_x \approx 0.15$. When working in the specified limit, these may be sufficient depending on the required precision. At higher i_x (or if precision better than $10^{-2} - 10^{-3}$ is required), however, the numerically obtained functions can prove to be useful as the fits no longer work very well.

We would like to comment on the surprising change of trend near $i_x = i_x^* \approx 0.212$ in $\Delta\mu(i_x)$ on Fig.3(a,b) and the lack thereof on $-\Delta i_x(i_x)$ in Fig.4(a,b). The decrease of both with the growth of i_x from 0 to i_x^* is not surprising, since the part of the trajectory to the right of the *uncertainty curve* is the most subject to radiation losses. We believe the slight increase in $\Delta\mu$ at $i_x > i_x^*$ is due to the fact that near the uncertainty curve the trajectory of the particle in the "fast" phase space is close to the separatrix, so the particle is less subject to radiation reaction [22], or, in mathematical terms, $x^2 \approx 0$ in Eq.12 or $\eta \approx \cos\varphi(\eta) \approx -1$ in Eq.17. As a result, the increase is noticeable, but still rather slight. For $\Delta i_x(i_x)$, however, the factor $f'(-\eta)$ in (20-21) mitigates this, since for trajectories close to the center of the "slow" phase space (Fig.2, $i_x \approx i_{xmax}$) $f'(-\eta) \approx 0$ as the phase space center corresponds to $\eta = \eta^*$ [22].

A special note should be made about the obtained form of the function $L(i_x)$. Since it is obtained via integrating $\Delta\mu/\Delta i_x$ (27), and those two functions, in turn, are calculated in some number of discrete points, there is an additional risk of a numerical integration error, which in this case may accumulate over i_x . The integral $\int_0^{i_{xmax}} -\Delta\mu/\Delta i_x dx$ diverges to infinity on both sides. Near $i_x = 0$ the rather precise approximation $-\Delta\mu/\Delta i_x \approx 2/i_x$ and the free constant of integration allow us to calculate the first few points alternatively to integration, but there is no accurate fit near $i_x = i_{xmax}$, so the issue especially important in this region. We note that the accuracy of the fit near $i_x = i_{xmax}$ on Fig.6d (in red) represents the discrepancy between the red curve on Fig.6b (rough fit) and the blue curve (numerically integrated using Eq. 27), so it does not take into account the integration error described in this paragraph. While we have done our best to calculate $L(i_x)$ accurately, an analytically derived fit near $i_x = i_{xmax}$ would help to alleviate this problem.

IV. DISCUSSION

The method of slowly changing parameters was used to quantify the influence of radiative friction over a single half-period $T_y/2$. The obtained expressions and the performed numerical calculations can be used to evaluate the changes of key parameters μ and i_x over $T_y/2$, to employ the obtained invariant $L(\mu, i_x)$ or to construct a system of differential equations describing the system on long timescales $\Delta t \gg T_y$. This system is much easier to analyze on the specified timescales than the original one (2), because, first, it is a system of only two differential equations instead of five or six, and second, one would need to resolve only the time scales $\mu/\dot{\mu}$ and i_x/\dot{i}_x instead of T_x , which is at least two orders of magnitude lower (14).

Additionally, while we used the method of slowly changing parameters to calculate the according functions in the assumptions described in Sec.III, it can be applied to a more general problem, where some of these assumptions can be completely or partially lifted.

The second term in (12) corresponding to B_x does not have to be neglected. Proper calculations would entail somewhat more intricate math, but the method perfectly applies. However, the condition for weakness of B_x [7] is required in order to be able to describe trajectories with the model described in Sec.II in the first place.

The requirement of ultrarelativity can be lifted: the problem can be considered in the general relativistic case. Then the third term of the radiative friction force in Eq.11 would need to be replaced with its full form [24], which would complicate the mathematics quite a bit, but the method still applies.

Finally and most interestingly, with some modifications to the method the requirement $T_y \ll \gamma/\dot{\gamma}, i_x/\dot{i}_x$ (14) can be lifted (but not $T_x \ll \gamma/\dot{\gamma}, i_x/\dot{i}_x$ or $T_x \ll T_y$). In this case differential equations for μ and i_x have to be solved self-consistently alongside with the one for q_y . An important note is that in this case Eq.20 stands and, considering η in the form (16), the variables μ and i_x can be separated. Therefore, the equation can be integrated to find a new invariant $L(\mu, i_x, q_y)$ valid on time scales $\Delta t \leq T_y$. The exact form of this invariant is, however, outside the scope of this paper.

We note that although technically the presented method can be used with all of these assumptions lifted simultaneously, it would require immense analytical and computational efforts. Therefore, we remind that one should attune to the problem at hand and lift only those assumptions that truly require doing so.

Lastly, the effect of quasirandom jumps of the quasiadiabatic invariant of nondissipative motion i_x [7] in the vicinity of the uncertainty curve were ignored in this work. Since they occur in a close vicinity of the uncertainty curve during time intervals $\Delta t \ll T_y$, the change to μ during this time can be neglected. Therefore, the quasiadiabatic invariant of dissipative motion $L(\mu, i_x)$ will experience jumps according to the jumps in i_x , which

have been extensively studied before.

V. CONCLUSION

The motion of an ultrarelativistic particle experiencing radiative friction in null current sheets with a two-component magnetic field (with a weak component perpendicular to the sheet) was considered. The method of slowly changing parameters was used to quantify the influence of weak radiation reaction considered in the form of the continuous Landau-Lifshitz force on key parameters defining the dynamics of the particle. The expressions quantifying this influence were found, and due to their intricacy they were nondimensionalized and com-

puted numerically. A quasiadiabatic invariant of dissipative motion was found and also computed numerically in dimensionless variables. Theoretical fits were tested, their precision analyzed depending on the value of key parameters, and in some cases more precise fits were found numerically.

It was also shown how the presented method can be applied in a wider range of problems where some of the employed assumptions are completely or partially lifted.

ACKNOWLEDGMENTS

The work was supported by the Foundation for the Advancement of Theoretical Physics and Mathematics "BASIS".

-
- [1] N. F. Ness, *J. Geophys. Res.* **70**, 2989 (1965).
 [2] T. W. Speiser, *J. Geophys. Res.* **70**, 4219 (1965).
 [3] T. W. Speiser, *J. Geophys. Res.* **72**, 3919 (1967).
 [4] B. U. Ö. Sonnerup, *J. Geophys. Res.* **76**, 8211 (1971).
 [5] J. Büchner and L. M. Zelenyi, *J. Geophys. Res.: Sp. Phys.* **94**, 11821 (1989).
 [6] L. M. Zelenyi, H. V. Malova, A. V. Artemyev, V. Y. Popov, and A. A. Petrukovich, *Plasma Phys. Rep.* **37**, 118–160 (2011).
 [7] L. M. Zelenyi, A. I. Neishtadt, A. V. Artemyev, D. L. Vainchtein, and H. V. Malova, *Phys. Usp.* **56**, 347 (2013).
 [8] L. M. Zelenyi, H. V. Malova, E. E. Grigorenko, and V. Y. Popov, *Phys. Usp.* **59**, 1057 (2016).
 [9] J. Arons, *Space Science Reviews* **173**, 341 (2012).
 [10] E. S. Efimenko, A. V. Bashinov, S. I. Bastrakov, A. A. Gonoskov, A. A. Muraviev, I. B. Meyerov, A. V. Kim, and A. M. Sergeev, *Scientific Reports* **8**, 2329 (2018).
 [11] A. A. Muraviev, S. I. Bastrakov, A. V. Bashinov, A. A. Gonoskov, E. S. Efimenko, A. V. Kim, I. B. Meyerov, and A. M. Sergeev, *Jetp Lett.* **102**, 148 (2015).
 [12] C. N. Danson, C. Haefner, J. Bromage, T. Butcher, J.-C. F. Chanteloup, E. A. Chowdhury, A. Galvanauskas, L. A. Gizzi, J. Hein, D. I. Hillier, and et al., *High Power Laser Science and Engineering* **7**, e54 (2019).
 [13] A. Gonoskov, A. Bashinov, I. Gonoskov, C. Harvey, A. Ilderton, A. Kim, M. Marklund, G. Mourou, and A. Sergeev, *Phys. Rev. Lett.* **113**, 014801 (2014).
 [14] A. Bashinov, A. Gonoskov, A. Kim, G. Mourou, and A. Sergeev, *Eur. Phys. J. Spec. Top.* **223**, 1105 (2014).
 [15] L. L. Ji, A. Pukhov, I. Y. Kostyukov, B. F. Shen, and K. Akli, *Phys. Rev. Lett.* **112**, 145003 (2014).
 [16] N. Neitz and A. Di Piazza, *Phys. Rev. Lett.* **111**, 054802 (2013).
 [17] Y. B. Zel'dovich, *Sov. Phys. Usp.* **18**, 79 (1975).
 [18] S. V. Bulanov, T. Z. Esirkepov, J. Koga, and T. Tajima, *Plasma Phys. Rep.* **30**, 196 (2004).
 [19] J. G. Kirk, *Pl. Phys. Contr. Fusion* **58**, 085005 (2016).
 [20] E. Gelfer, N. Elkina, and A. Fedotov, *Sci Rep* **8**, 6478 (2018).
 [21] C. H. Jaroschek and M. Hoshino, *Phys. Rev. Lett.* **103**, 075002 (2009).
 [22] A. Muraviev, A. Bashinov, E. Efimenko, A. Gonoskov, I. Meyerov, and A. Sergeev, *Phys. Rev. E* **104**, 065201 (2021).
 [23] A. Runov, R. Nakamura, W. Baumjohann, R. A. Treumann, T. L. Zhang, M. Volwerk, Z. Vörös, A. Balogh, K.-H. Glaßmeier, B. Klecker, H. Rème, and L. Kistler, *Geophysical Research Letters* **30** (2003).
 [24] L. D. Landau and E. M. Lifshitz, *The Classical Theory of Fields* (Elsevier, Oxford, 1975).
 [25] This expression can also be derived by the same logic as in [7] for the parameter s (or $-\eta$), with a remark that the Hamiltonian can only be divided into terms associated with the motion in the (x, y, z) direction due to the conservation of the common Lorentz-factor γ , and that these terms no longer directly represent the kinetic energy.
 [26] Both p_y and q_y will be used throughout the paper, but in most arguments they are interchangeable.
 [27] The ambiguity due to the sign of q_y will be addressed later.
 [28] $f_{max} \approx 1.547$ is the maximal value of $f(s)$. The value i_x for the trajectory tangent to the *uncertainty curve* can be found by setting $q_y = 0$ and $\eta = -1$ in (9).